^{13}C and ^{39}K High-Resolution Solid-State NMR Study of the Nonferroic Phase Transition of Potassium Hydrogen Carbonate. Complementarity between NMR and Incoherent Neutron Scattering

Christophe Odin*

Groupe Matière Condensée et Matériaux, UMR6626 au CNRS, Université Rennes I, Campus de Beaulieu, 35042 Rennes Cedex, France

Received: October 23, 2003; In Final Form: February 16, 2004

Potassium hydrogen carbonate $KHCO_3$ is formed of centrosymmetric dimers $(HCO_3^-)_2$ linked by hydrogen bonds, the protons being disordered in an asymmetric double-well potential at ambient temperature. This compound is a model for 0-dimensional hydrogen bonds. It undergoes a nonferroic nonferroelectric phase transition at $T_c = 318$ K, and the double-well potential becomes symmetric in the high-temperature phase. This phase transition is studied *for the first time* by variable-temperature ^{13}C and ^{39}K high-resolution solid-state NMR experiments. We present an original method to correlate NMR data to other local probes such as incoherent neutron scattering experiments to extract structural information from powder NMR experiments. Using this method, the eigenvalues and jump angle of the chemical shift tensor of the carbon ^{13}C and the quadrupolar interaction of the potassium ^{39}K could be extracted in the completely ordered phase, and their evolution with temperature is correlated to the proton-dynamic disorder within the hydrogen bond. This study also illustrates the complementarity between NMR and incoherent neutron-scattering experiments in the study of hydrogen bonding.

Introduction

The hydrogen carbonate $XHCO_3$ family with (X = Na, K, Rb, Cs) is interesting in the context of both supramolecular engineering and hydrogen bond (HB) studies because it gives a series of ionic compounds with hydrogen-bonded dimers (rings) with the notable exception of $NaHCO_3$, which forms infinite chains of HB. Moreover, potassium hydrogen carbonate $KHCO_3$ is known to undergo different phase transitions as a function of temperature,[1,2] stress,[3−6] or hydrostatic pressure.[7] Thus, this family gives the opportunity to analyze in detail the competition between ionic and hydrogen bonding, the structure and dynamics of hydrogen bonds, as well as phase transitions connected to hydrogen disorder in HB. This family is also well suited for NMR studies because all nuclei except oxygen (if not enriched in $^{17}0$) can be studied with reasonable sensitivity.

Potassium hydrogen carbonate $KHCO_3$ appears to be a good model for the study of 0-dimensional hydrogen bonds.[8−15] The dianions $(HCO_3^-)_2$ form centrosymmetric dimers linked by two adjacent hydrogen bonds, and the protons are disordered in a double-minimum potential as evidenced by RX and neutron experiments.[4,16] At room temperature and down to 14 K, the crystal has a monoclinic $P2_1/a$ structure[15,16] with two formula units ($K^+HCO_3^-$) per unit cell (Figure 1a): the long principal axis of the dimers are tilted antiphase at the corner and the center sites of the (*a*,*b*) plane when viewed in a *c*-projection, the protons being disordered in an asymmetric double-well potential. This ionic nonferroelectric compound undergoes a structural phase transition at $T_c = 318$ K to a monoclinic $C2/m$ high temperature (HT) phase with one formula unit ($K^+HCO_3^-$) per unit cell.[2] In the high-temperature phase, there is no tilt of the dimers (Figure 1b), at least on average, and the double-well potential becomes symmetric, as proven by incoherent neutron-scattering experiments.[17] The isotope effect on the transition temperature which changes from $T_c(H) = 318$ K to $T_c(D) = 353$ K for, respectively, the hydrogenated and deuterated samples points out the role of the hydrogen bond on the mechanism of the phase transition.

Among the different experimental techniques to study proton stochastic disorder, high-resolution NMR and incoherent neutron scattering are complementary (see, for instance, ref 18). Incoherent neutron scattering measures mainly the spatial and temporal autocorrelation function of the proton and gives information about the geometry of the proton trajectory, as well as its dynamics down to a resolution of a few GHz in the best cases. For longer time scales, the high versatility of high-resolution solid-state NMR with respect to the choice of the time-scales, its very high selectivity concerning the nucleus to be probed which provides accurate description of its local environment, and easy in-laboratory access make of NMR a very efficient tool in providing fundamental information about phase transitions. It is also particularly adapted for probing the motional dynamics of protons in hydrogen bond compounds as well as its local environment.[19,20] For instance, the spectral density of the proton dynamics is probed through dipolar interaction at the proton Larmor frequency by spin−lattice relaxation times measurement.

The understanding of the role of hydrogen bonding on the chemical-shielding tensors of carbons ^{13}C in carboxylic groups is important to separate the different contributions coming from the local electronic structure and geometry, bond lengths, proton disorder, and dynamics...for instance, to predict molecular or macromolecular conformations from NMR measurements. Usually, general trends are obtained by correlating the chemical shift anisotropy (CSA) eigenvalues of different compounds to the different structural available data such as bond lengths and

* Fax: (33) 02 23 23 67 17. E-mail: christophe.odin@univ-rennes1.fr.

10.1021/jp037206h CCC: $27.50
Published on Web 05/04/2004

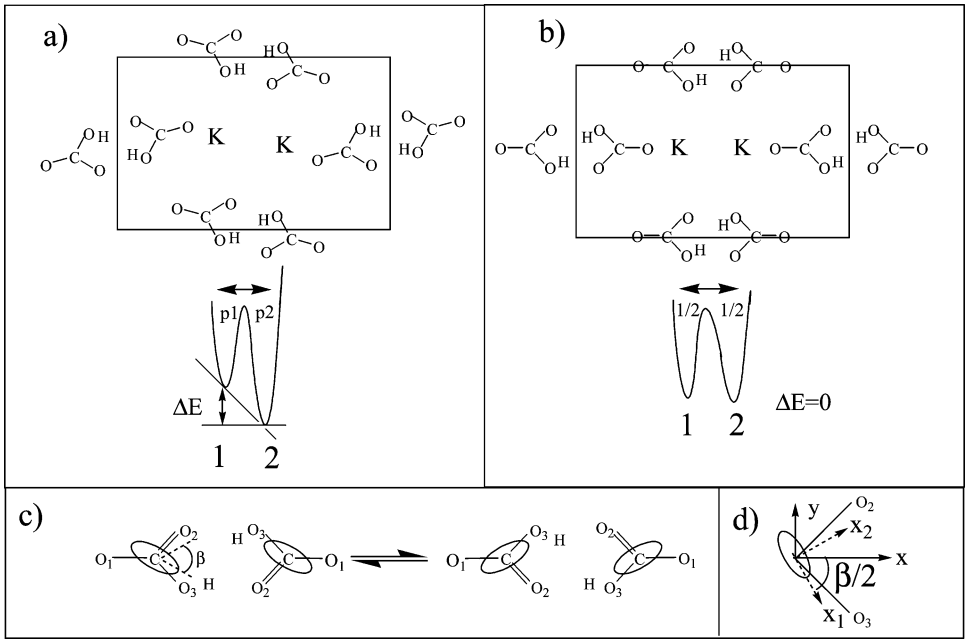

Figure 1. Schematic drawing of the two phases of $KHCO_3$ in the (a,b) plane: (a) low-temperature phase; (b) high-temperature phase. The double-well potential represents a "two-pocket state" approximation of the real multidimensional potential energy surface. The abscissa is an effective reaction coordinate. (c) Schematic of the two tautomeric forms of the cyclic dimer. The ellipse around the carbon mimics the orientation (arbitrary here) of the chemical shift tensor. The principal direction x_3 corresponding to the most shielded component is assumed to be perpendicular to the plane of the dimer. (d) Definition of the jump angle $\beta/2$ where the x axis bisects the $\angle CO_2O_3$ angle in the HT phase and the z axis is perpendicular to the plane of the donor/acceptor oxygens.

angles.[21−23] But only a few experiments take into account the influence of the proton dynamical disorder which can average the carbon chemical shift tensor. A rare example is benzoic acid where the influence of the proton disorder on the carbon averaged CSA tensor was studied at different temperatures.[24−26]

In the family $XHCO_3$, the different nuclei give complementary information at different spatial and time scales depending on the type of interaction. Hydrogen or deuterium directly probe the hydrogen bond and its dynamic disorder through, respectively, dipolar coupling or quadrupolar interaction. The cations are all quadrupolar nuclei of spin $I = {}^3/_2$, and they probe the electric field gradient tensor $(\partial^2 V)/(\partial x_i \partial x_j)$ at the nucleus. We expect this interaction to be very sensitive to both the ionic character of the sample and subtle changes in electronic densities or charge distributions. Finally, the carbon chemical shift tensor is very sensitive to the local electronic structure.[27] The stochastic concerted jump of the protons of the hydrogen bonds between the two minima of the asymmetric double-minimum potential mediates the conversion between two tautomers (Figure 1c). The carbon chemical shift tensor probes then the proton ordering through the coupling of the electronic structure of the donor and acceptor oxygens to the dynamic disorder of the proton in the hydrogen bond. The nonferroic phase transition of $KHCO_3$ offers the unique opportunity to study the variation of the ^{13}C and ^{39}K interaction tensors as a function of proton dynamical disorder because of the change from a symmetric to an asymmetric double-well potential whose energy difference can be controlled by temperature.

Some NMR/NQR experiments were performed on $KHCO_3$. To our knowledge, only one article refers explicitly to the nonferroic phase transition, namely to explain the proton spin−lattice relaxation behavior as a function of temperature.[28] The other articles did not consider the phase transition because its existence was not known at that time (the monoclinic/monoclinic phase transition was discovered by Haussühl in 1986). The proton chemical shift tensor was measured at ambient temperature.[29] The potassium quadrupolar coupling constant at ambient temperature was estimated by NQR.[30] The anisotropy of the Zeeman spin−lattice relaxation time of deuterium in $KDCO_3$ was studied between 77 and 300 K,[31] and the asymmetry and potential barrier of the double-well potential were deduced from these results. Oxygen NQR experiments were also performed.[32,33] In fact, a collapse of the two sets of ^{17}O quadrupole resonance frequencies was observed by Larcombe−McDoual and Smith[33] at 341 K and interpreted using a double-well potential whose asymmetry diminishes as the temperature rises. But this was not attributed to a phase transition.

This paper is organized as follows. First, we present *the first study* of the nonferroic phase transition of $KHCO_3$ by ^{13}C (spin $I = {}^1/_2$) and ^{39}K (spin $I = {}^3/_2$) high-resolution NMR experiments by studying the powder line shapes as a function of temperature in the range $200 \leq T \leq 340$ K. Second, we revisited the two-site jump model to propose a method to obtain the static eigenvalues and the jump angle from powder experiments by correlation with results from other local probes, as well as some geometric indications. Third, this method is used for the chemical shift tensor of carbon and for the quadrupolar interaction tensor of potassium in $KHCO_3$ by correlating our NMR data to incoherent neutron scattering results. The results are discussed in view of the general trends of the influence of hydrogen bonding on ^{13}C chemical shift tensors, both for the eigenvalues but also for the local orientation of the CSA principal axes.

Experimental Section

Potassium hydrogen carbonate powder $KHCO_3$ were purchased from Fluka (99.7% purity) and used to fill the rotors without purification.

All the spectra were acquired with a Bruker ASX 300 spectrometer with a Bruker CP/MAS probe which drives

zirconium oxide rotor of 4 mm. The temperature was regulated with the corresponding temperature unit VT2000.

The CP or CP/MAS ^{13}C experiments at Larmor frequency 75.48 MHz were performed with the usual cpmas sequence, employing high-power CW proton decoupling during acquisition. The proton P90 pulse width was in total 3.5 μs, the optimized contact time of 5 ms, and a recycle time of at least 300 s because of the long proton relaxation time. No study of the proton relaxation time as a function of temperature was attempted, but the consistency of the spectra was verified by using different recycle times. The ^{13}C chemical shifts were referenced to TMS. Typically, 16 and up to 800 transients were accumulated for, respectively, MAS and quasistatic experiments.

To estimate the errors in the eigenvalues of the carbon chemical shift tensor, two types of experiments were performed: CP/MAS experiments at a rotation frequency of $\nu_R = 1250 \pm 3$ Hz and quasistatic experiments at ~50 Hz because our laboratory has no double-resonance static probe. Since the temperature is regulated by the bearing air flux (the air flux which supports the rotor) in the Bruker CP/MAS probe, it is not possible to perform true static experiments with this CP/MAS probe except at ambient temperature with no air flux and no temperature regulation. To circumvent the problem, we used a modified rotor which rotates at approximately ~50 Hz when the bearing air flux was set at the same value as the one used for a $\nu_R = 1250$ Hz rotation frequency. Moreover, it was very difficult to reach very low temperature because of freezing problems, even by using two additional water nitrogen sinks to dry the air after the air-dryers furnished by the normal MAS installation. We found that the problem comes mainly from the loss of the regulation signal used to keep the rotation frequency of the rotor stable within a few hertz (usually ± 3 Hz) because the optical fiber is too close to the bearing air tube. It was verified at ambient temperature that the true static spectrum and the corresponding quasistatic spectrum are identical within the experimental errors.

The spectra of the second-order quadrupolar perturbed central transition ($+1/2 \leftrightarrow -1/2$) of the potassium ^{39}K ($I = 3/2$) at Larmor frequency 14.01 MHz were acquired with a monocanal Bruker static probe with an air flux temperature regulation. We used the same experimental air-flux setup as in the MAS experiments. The pulse sequence was a Hahn echo(θ) $-$ τ $-$ (2θ) $-$ *acq* with a 16-phase cycle, a typical pulse length of $\theta = 7$ μs, a refocalization delay of $\tau = 80$ μs, and a recycle time within 0.5−3 s. Depending on temperature, a number of 6k to 16k transients were collected to obtain an acceptable signal-to-noise ratio.

All the spectra were fitted using the program WINFIT.[34]

Results and Discussion

^{13}C and ^{39}K Variable-Temperature Solid-State NMR on $KHCO_3$. Since the low- and high-temperature phases of $KHCO_3$ are known from crystallographic studies, we can draw some conclusions about the different types of NMR spectra we expect to observe on the basis of symmetry considerations. Potassium hydrogen carbonate $KHCO_3$ is monoclinic in both the high- and low-temperature phases, with, respectively, one and two dimers per unit cell. In the LT and HT phases, the two carbons of each dimer are magnetically equivalent because they are linked by a center of inversion, so NMR cannot distinguish between them. In the LT phase, the chemical shift tensors (CST) of the carbons of the two differently oriented dimers should have the *same set of principal values* because they are related by the monoclinic glide plane. But since the orientations of the principal axes of the CST are different except for particular orientations of the static magnetic field, two lines are expected in a high-resolution solid-state NMR spectrum of a single crystal for the LT phase, and only one line in the HT phase where the two dimers become equivalent. However, because a powder NMR spectrum is only sensitive to the *eigenvalues* of the interaction tensors of the two magnetically inequivalent nucleus in the LT, there is *only one powder spectrum* because the eigenvalues of the two tensors are the same. As a consequence, powder NMR will measure a signature of the phase transition only if the eigenvalues of the interaction tensor of the nucleus under study are modified. These symmetry considerations also apply to the quadrupolar interaction tensor of potassium.

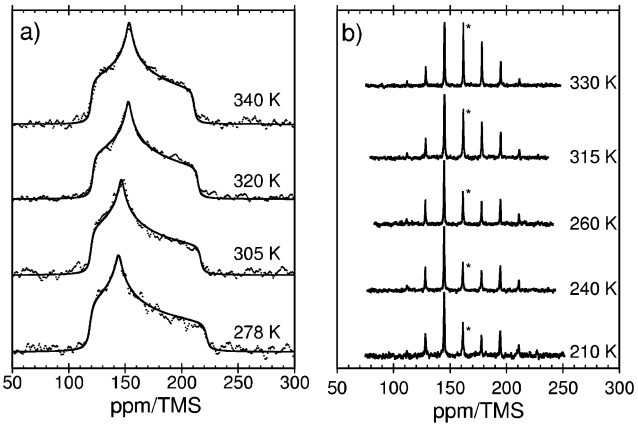

Figure 2. CP ^{13}C spectra of $KHCO_3$ at different temperatures. (a) Quasistatic CP spectra. The continuous gray lines are the best fit of the experimental data with a single site theoretical powder spectrum resulting from first-order chemical shift interaction. (b) CP/MAS spectra at $\nu_r = 1250$ Hz; the stars indicate the isotropic line.

^{13}C NMR of $KHCO_3$. We first consider the influence of the phase transition on the CST of the carbon ^{13}C. The quasistatic and MAS spectra at different temperatures in the range 210−340 K are presented in Figure 2a,b. Clearly, both types of spectra are different in the high-temperature (HT) and low-temperature (LT) phases. The experimental static powder spectra are well fitted with a single-site theoretical first-order powder line shape, in agreement with the previous symmetry considerations. From Figure 2a, it is seen that the smallest eigenvalue of the CSA is temperature independent within the experimental uncertainties. Also, the middle eigenvalue corresponding to the spectrum divergence decreases when temperature decreases below the critical temperature, whereas the largest eigenvalue increases. On the other hand, the MAS spectra (Figure 2b) indicate that the isotropic chemical shift varies slightly, if at all, with temperature.

We quantified the corresponding isotropic chemical shift δ_{iso}, the anisotropy parameter δ_{eff}, and the asymmetry parameter η_{eff} by fitting the experimental spectra. From these experimental values, the eigenvalues are obtained. In the convention we use, the eigenvalues of the CST are arranged such that $\delta_{11} > \delta_{22} > \delta_{33}$ and related to δ_{iso}, δ_{eff} and η_{eff} by the following relationships:

$$\delta_{11} = \delta_{iso} + \delta_{eff} \tag{1}$$

$$\delta_{22} = \delta_{iso} - \frac{\delta_{eff}}{2}(1 - \eta_{eff}) \tag{2}$$

$$\delta_{33} = \delta_{iso} - \frac{\delta_{eff}}{2}(1 + \eta_{eff}) \tag{3}$$

The subscript eff (effective) was added to the anisotropy and asymmetry parameter to stress that they are temperature-

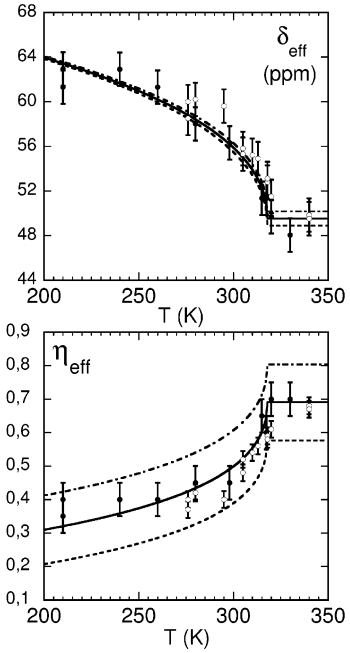

Figure 3. Effective anisotropy δ_{eff} and asymmetry η_{eff} parameters of the ^{13}C CSA tensor of $KHCO_3$ as a function of temperature. Solid symbols refer to the MAS experiment, whereas open symbols refer to the static experiment. The lines were calculated with a two-site jump model as explained in the text with $\delta = 67$ ppm, $\beta = 52°$. Three different initial asymmetry parameters were used: $\eta = 0.25$ (continuous line) and $\eta = 0.15$ (dashed line) or $\eta = 0.35$ (dash−dot line).

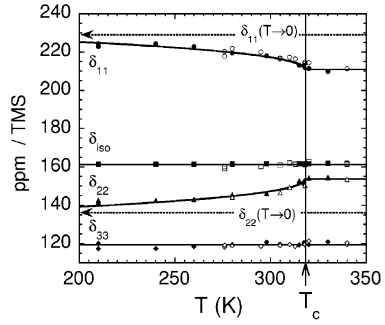

Figure 4. Evolution of the eigenvalues of the CSA tensor of ^{13}C as a function of temperature. Solid symbols refer to the MAS experiment, whereas open symbols refer to the static experiment. At this scale, the error bars are of the order of the marker sizes. The continuous lines represent the expected temperature evolution obtained from the two-site jump model, as explained in the text ($\delta = 67$ ppm, $\eta = 0.25$ and $\beta = 52°$). The two horizontal lines indicate the estimated values of δ_{11} and δ_{22} in the ordered state.

dependent quantities. We keep the notations δ and η for the anisotropy and asymmetry parameter of the chemical shift tensor *with no proton jump* (see infra).

The results are presented in Figures 3 and 4 as a function of temperature. Upon increasing temperature, the anisotropy parameter δ_{eff} strongly decreases from ~64 ppm at the lowest temperature to ~50 ppm in the HT phase. At the same time, η_{eff} is doubled from ~0.35 to 0.7 (Figure 3). We found the transition temperature consistent with the accepted value of $T_c = 318$ K. The isotropic part of the chemical shift is constant within our experimental resolution: $\delta_{iso} \approx 161$ ppm with a standard deviation $\sigma \approx 1$ ppm (Figure 4). The most shielded component is also a constant $\delta_{33} \approx 119$ ppm with a standard deviation $\sigma \approx 1$ ppm. Since δ_{33} is constant, it means that the product $\delta_{eff}(1 + \eta_{eff})$ is independent of temperature. Therefore, the occurrence of the phase transition is only reflected by the

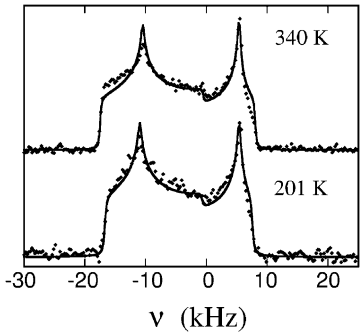

Figure 5. Static second-order quadrupolar spectra of the central transition ($-1/2 \leftrightarrow 1/2$) of the $I = 3/2$ nucleus ^{39}K in the HT and LT phases of $KHCO_3$. The continuous lines are the best fit of the experimental data obtained with the theoretical powder line shape using only quadrupolar interaction at second order and neglecting chemical shift anisotropy effects.

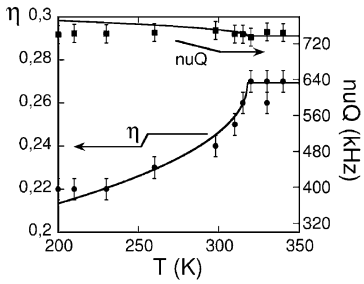

Figure 6. Effective quadrupolar interaction nuQ and asymmetry η parameter of the potassium ^{39}K quadrupolar tensor as a function of temperature. Note the different scales on the right and left sides. The continuous lines were calculated as explained in the text with nuQ =780 kHz, $\eta = 0.2$, and $\beta = 22°$.

changes in the least shielded and medium shielded eigenvalues δ_{11} and δ_{22}, the decrease of δ_{11} with temperature reflecting the corresponding decrease of the apparent strength of the chemical shift interaction δ_{eff}. The invariance of both δ_{iso} and δ_{33} has the consequence that $\delta_{11} + \delta_{22} =$ cste, as verified experimentally. The consequences of these results will be discussed in detail in the following text.

^{39}K Second-Order Quadrupolar NMR of $KHCO_3$. Static ^{39}K ($I = 3/2$) NMR quadrupolar spectra in the LT and HT phases are presented in Figure 5. These spectra correspond to the powder line shape of the central transition ($+1/2 \leftrightarrow -1/2$) perturbed by second-order quadrupolar interaction. The agreement between the experimental spectra and the theoretical powder line shape is excellent, indicating that the effect of the CSA of the potassium could be neglected. These fits permit the extraction of the quadrupolar coupling constant $nuQ_e = eV^e_{zz}Q/2h$ and the asymmetry parameter $\eta_{eff} = (V^e_{xx} - V^e_{yy})/V^e_{zz}$ as a function of temperature (Figure 6). $V^e_{\alpha\alpha}$ denotes the eigenvalues of the electric field gradient (EFG). Given the error bars, the quadrupolar coupling constant shows little variation with temperature, and its average is nuQ = 743 kHz with a standard deviation of 5 kHz. Such a value is consistent with the value obtained by Poplett[30] who measured $(eV_{zz}Q/2h)(1 + \eta^2/3)^{1/2} \approx 758$ kHz at room temperature. The effect of the phase transition is mainly reflected by the evolution of the asymmetry parameter η_{eff}, which increases from 0.22 to 0.27 where it saturates in the HT phase.

To summarize, both the chemical shift tensor of the carbon ^{13}C and the quadrupolar interaction tensor at the potassium site ^{39}K are affected by the phase transition. The main effect is a strong increase of the asymmetry parameter and a decrease of the anisotropy parameter when temperature is raised. Both

parameters saturate in the HT phase, so that the phenomenon is linked to a phase transition. It also indicates that the observed evolution is not a simple consequence of a "*normal*" motional averaging which would become more and more effective when temperature is increased.

By performing incoherent neutron scattering experiments on $KHCO_3$, Eckold[17] showed that the proton evolves in an asymmetric double-well potential in the LT phase. This double-well potential becomes symmetric in the HT phase. The order/disorder component of the phase transition is then described by the order parameter Δp which is the difference of occupation probability between the two sites of the double-minimum potential $\Delta p = p_1 - p_2$. All the physical quantities are thus expected to correlate with respect to the order parameter Δp. The stochastic concerted jump of the protons of the hydrogen bonds between the two minima of the asymmetric double-minimum potential mediates the conversion between two tautomers (Figure 1c). This stochastic jump modulates the NMR interaction tensors: the carbon CST through a modulation of the electronic densities of the donor and acceptor oxygens and the quadrupolar interaction tensor by a modulation of the local charge densities. From the NMR point of view, this stochastic modulation precludes from extracting the instantaneous interaction tensor linked to the minority and majority sites if the jump correlation time τ_c is fast enough to completely average the tensor on the NMR time scale, that is when τ_c is small compared to the inverse of the static line width ($\tau_c \Delta \ll 1$). Such a two-site jump model has been successful in interpreting the deuterium relaxation measurements in $KDCO_3$ in the low-temperature phase[31] and similar experiments in carboxylic acids[18,24−26] or other hydrogen-bond compounds.[35] It is important to stress that such a two-site jump model does not make any hypothesis about the nature (classical or quantum) and the dimensionality of the multidimensional potential energy surface (MPES) describing the states of the two tautomers. This is a "two-pocket state" approximation of the real MPES. It is fully justified in our analysis because our NMR results are not sensitive to the real shape of the MPES, but only to the difference of occupation probability between the two sites $\Delta p = p_1 - p_2$.

In the following, we show that the observed variations of the anisotropy and asymmetry parameters could be rationalized by invoking a dynamic average of the corresponding tensor due to the stochastic proton motion in an asymmetric double-well potential whose varying asymmetry depends on the phase-transition order parameter.

NMR and the Two-Site Jump Model Revisited. Although two-site jump processes are the simplest stochastic models in physics, they are nevertheless very important because they can be used as a first approach in modeling proton order/disorder in hydrogen bonding.

As a first approximation, the double-proton transfer switches stochastically the dimer between two tautomers, whose NMR interaction tensors are different. When the jump correlation time τ_c is small compared to the inverse of the static line width Δ ($\tau_c \Delta \ll 1$ and the static line width is typically the maximum span of both frequencies whatever the magnetic field orientation), the NMR line shape is governed by an averaged tensor. In this hypothesis of motional averaging, the averaged tensor for a two-site jump is

$$< T > = \frac{T_1 + T_2}{2} + \Delta p \frac{T_1 - T_2}{2} \tag{4}$$

where T_1 and T_2 are the interaction tensors for sites 1 and 2 of occupation probabilities $p_1 = (1 + \Delta p)/2$ and $p_2 = (1 - \Delta p)/2$.

To go further, we assume that tensors T_1 and T_2 possess the same principal values (i.e., are congruent). This is the case if the two sites are related by symmetry, as it should be for an order/disorder phase transition. In that case, the difference $\Delta p = p_1 - p_2$ can be interpreted as the order parameter of the phase transition.

We also need the relative orientation between the principal axes of the two tensors, which is generally defined by three angles. However, we found experimentally that the most shielded component δ_{33} of the carbon chemical shift tensor is independent of temperature. In appendix A, we prove the following important result. It is shown that *the only possibility* for an averaged tensor of the form of eq 4 to keep is lowest eigenvalue δ_{33} constant is that the average is performed between two tensors T_1 and T_2 having in common the corresponding principal axis x_3. As a consequence, the CSA data show that the two congruent tensors are related by a rotation of angle β around axis x_3, $T_2 = R^T_{x3}(\beta) T_1 R_{x3}(\beta)$, and we limit the analysis to this four-parameter (δ, η, Δp, β) case (Figure 1d).

The initial unaveraged tensor in its principal axis system (PAS) was chosen as a traceless tensor

$$T_1 = \mathrm{diag}\left(\delta, -\frac{\delta}{2}(1 - \eta), -\frac{\delta}{2}(1 + \eta)\right) \tag{5}$$

The isotropic contribution is not considered because it is evidently unaffected by the motion. The third component of the tensor corresponding to the rotation axis x_3 is also obviously not modified by the rotation.

At this point, we need to introduce the convention we use to characterize a traceless second-rank tensor, which depends on only two parameters (see also refs 36 and 37). In our case, the most convenient convention is to arrange the eigenvalues such that $\lambda_{xx} \geq \lambda_{yy} \geq \lambda_{zz}$ and to define the anisotropy parameter by $\delta_e = \lambda_{zz}$ and the asymmetry parameter by $\eta_e = (\lambda_{yy} - \lambda_{xx})/\lambda_{zz}$. The eigenvalues are then related to δ_e and η_e by the same equation as the one we used for the chemical shift tensor, eqs 1−3. It is possible to show that all possibilities can be covered if $\delta_e \geq 0$ and $0 \leq \eta_e \leq 3$. As compared to the "absolute value convention" where $|\lambda_{xx}| \leq |\lambda_{yy}| \leq |\lambda_{zz}|$, $\delta_a = \lambda_{zz}$ and $\eta_a = (\lambda_{xx} - \lambda_{yy})/\lambda_{zz}$<frx>, our convention avoids the change of the labeling of the principal axes when the anisotropy and asymmetry parameters are strong functions of external parameters (temperature, pressure...). The two conventions are equivalent when $0 \leq \eta_e \leq 1$. When $1 \leq \eta_e \leq 3$, we have the relationships $\delta_a = -\delta_e/2(1 + \eta_e)$ and $\eta_a = (3 - \delta_e)/(1 + \eta_e)$.

By diagonalizing $<T>$, we obtained the corresponding effective anisotropy parameter δ_{eff}

$$\delta_{eff} = \frac{\delta}{4}[(1 + \eta) + (3 - \eta)\Psi(\Delta p,\beta)] \tag{6}$$

and the corresponding effective asymmetry parameter η_{eff}

$$\eta_{eff} = \frac{3(1 + \eta) - (3 - \eta)\Psi(\Delta p,\beta)}{(1 + \eta) + (3 - \eta)\Psi(\Delta p,\beta)} \tag{7}$$

where the Ψ function is defined as

$$\Psi(\Delta p,\beta) = \sqrt{\cos^2\beta + \Delta p^2 \sin^2\beta} \tag{8}$$

The definitions of δ_{eff} and η_{eff} were chosen to recover the initial values δ and η when the jump is frozen $|\Delta p| = 1$. As expected, the form of the variation of δ_{eff} and η_{eff} as a function

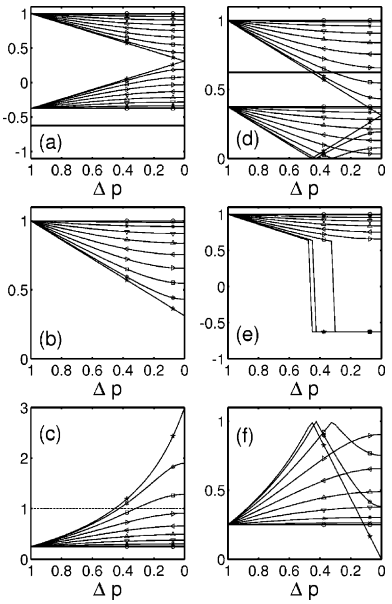

Figure 7. Variation of the eigenvalues (a), absolute value of the eigenvalues (d), and the corresponding anisotropy (b and e) and asymmetry parameters (c and f) in the two conventions described in the text (left, convention used in this work; right, absolute value convention), as a function of the order parameter $|\Delta p|$. The jump angle β varies between 0 and 90° by steps of 10° (some markers $\beta =$: 0°-(○), 50°(△), 90°(★)). The asymmetry parameter when $|\Delta p| = 1$ is $\eta = 0.25$. The sudden changes in the curves of δ_a and η_a are observed when η_e becomes larger than unity. At these points, the labeling of the 1 and 3 principal axes are interchanged to comply with the convention of ordering in absolute value.

of Δp only depends on β and η. δ does not change the shape, but only the scales of δ_{eff}.

It is interesting to study the bounds of δ_{eff} and η_{eff}. Note that for the completely ordered phase $\Psi(\pm 1,\beta) = 1$, whereas in the fully disordered phase $\Psi(0,\beta) = |\cos\beta|$. Whatever the values of Δp and β, it is easy to see that Ψ varies in the following range

$$0 \le |\Delta p| \le \Psi(\Delta p,\beta) \le 1 \tag{9}$$

Obviously, the lowest bound is attained when $\beta = \pi/2$, and the highest bound for $\beta = 0$. As a consequence, the effective anisotropy and asymmetry parameters are bounded:

$$\frac{\delta}{4}[(1+\eta) + (3-\eta)|\Delta p|] \le \delta_{\text{eff}} \le \delta \tag{10}$$

$$\eta \le \eta_{\text{eff}} \le \frac{3(1+\eta) - (3-\eta)|\Delta p|}{(1+\eta) + (3-\eta)|\Delta p|} \le 3 \tag{11}$$

These bounds imply that the *nonaveraged* asymmetry and anisotropy parameters verify $\eta \le \text{Min}(\eta_{\text{eff}})$ and $\delta \ge \text{Max}(\delta_{\text{eff}})$. If we say that disorder increases when the jump angle increases or when the order parameter decreases, then the effective anisotropy and asymmetry parameters are respectively decreasing and increasing functions of disorder. This is illustrated by Figure 7 for $\eta = 0.25$ with the two conventions for ordering the eigenvalues. As can be seen, the interpretation of the curves in the "absolute value ordering" convention is less intuitive because of sudden jumps of δ_a and non-monotonic behavior of η_a due to the necessity to relabel the different eigenvalues.

This two-sites jump model depends on four parameters (δ,η) and (Δp,β). In principle, the knowledge of the low-temperature asymmetry and anisotropy parameters δ and η when the order parameter is completely saturated ($\Delta p = \pm 1$) and of the corresponding data in the high-temperature phase ($\Delta p = 0$) are sufficient to predict the jump angle β. It can also be calculated from the combination of the HT values of the *effective* anisotropy and asymmetry parameter in the HT and of the corresponding values at a temperature where the order parameter is known, for instance when it can be measured by another experimental technique.

To this aim, it is convenient to define the function F as

$$F(\Delta p,\beta) = \delta_{\text{eff}}(3 - \eta_{\text{eff}}) = \delta(3-\eta)\Psi(\Delta p,\beta) \tag{12}$$

This function represents twice the difference between the largest and middle eigenvalues. The square of the ratio of this F function with its HT value ($\Delta p = 0$) defines the G function

$$G(\Delta p,\beta) = \frac{F(\Delta p,\beta)^2}{F(0,\beta)^2} = 1 + \tan^2(\beta)\Delta p^2 \tag{13}$$

This G function has the interesting property that it only depends on the jump angle β and on the square of the order parameter, *whatever the values of* δ *and* η. Moreover, it is a linear function of the square of the order parameter Δp^2 with slope $\tan^2(\beta)$. Thus, $t = \tan^2(\beta)$ can be readily estimated by linear least-squares fitting from the knowledge of at least two values, or more, of the order parameter. The other parameters δ and η of the static tensor can then be deduced from the experimental values of $A = F(0,\beta)(= \delta(3-\eta)|\cos\beta|)$ and $B = \delta(1+\eta)$ from the following formula:

$$\eta = \frac{3-C}{1+C} \tag{14}$$

where

$$C = \sqrt{1+t}\,\frac{A}{B}$$

and

$$\delta = \frac{1}{4}[B + A\sqrt{1+t}] \tag{15}$$

The uncertainties for β, η, and δ can be estimated by assuming that t, A, and B are independent quantities, using usual error propagation rules.

Correlation between NMR and Incoherent Neutron Scattering To Extract NMR Parameters with No Proton Disorder. In this part, we would like to show that once the variation of the order parameter as a function of temperature is known, we can extract the NMR parameters of the unaveraged tensors.

In hydrogenous systems, the total scattering is mainly dominated by the incoherent scattering of *protons* because the proton incoherent scattering cross-section is much larger than all the others. This fact makes incoherent neutron scattering an ideal method for studying proton disorder in hydrogen bonds. Moreover, it is usually considered as a more direct method than NMR because it involves less data reduction and modeling.

The Incoherent scattering function, neglecting the Debye−Waller factor and inelastic scattering, can be written as[38]

$$S_{\text{incoh}}(\mathbf{Q},\omega) \sim A(\mathbf{Q})\delta(\omega) + (1 - A(\mathbf{Q}))\,L(\mathbf{Q},\omega) \tag{16}$$

The first term is the elastic contribution, and $A(\mathbf{Q}) = |\langle e^{i\mathbf{Q}\cdot\mathbf{r}}\rangle|^2$ is called the Elastic Incoherent Scattering Factor (EISF). The brackets, $< >$, indicate an average over the probability density of the trajectory. So, the EISF is nothing more than the square

of the modulus of the spatial Fourier transform of the density probability of the trajectory, and it provides information about the geometry of the proton motion. The second term, the quasielastic part, contains information about the dynamics (time constants, etc.). If the nucleus jumps between two sites $\pm$ **a** with occupation probabilities $(1 \pm \Delta p)/2$, it is easy to show that the corresponding EISF is $A(\mathbf{Q}) = \cos^2(\mathbf{Q}.\mathbf{a}) + \Delta p^2 \sin^2(\mathbf{Q}.\mathbf{a})$. A measure of the EISF as a function of **Q** directly gives **a** and the square of the order parameter Δp^2. The quasielastic contribution $L(\mathbf{Q},\omega)$ is a Lorentzian whose width depends on the inverse of the jump correlation time τ_c.

Eckold investigated the nonferroic phase transition of $KHCO_3$ by incoherent neutron scattering,[17] and we summarize the main results. First, the square of the order parameter Δp^2 as a function of temperature was directly measured with the EISF, and it shows that the proton is not completely ordered at the lowest temperature (210 K) we could reach. So, the eigenvalues of the initial tensor are unknown and we had to use the method we proposed above to extract the unaveraged properties of the NMR interaction tensors. For convenience in the following data reduction, we have chosen to fit the square of the order parameter in the range 200 K up to the transition temperature and found that its temperature variation can be well reproduced by the following function: $\Delta p^2 \approx 1.3(1 - T/T_c)^{0.5}$. The value of the exponent here has no real significant physical meaning since it is evaluated from a very large range of temperatures. Second, from the quasielastic scattering function, the proton jump correlation time was found to obey an Arrhenius law $\tau_c = \tau_o e^{E_a/kT}$ with $\tau_o \approx 5 \times 10^{-13}$ s and an activation energy of $E_a = 42$ meV. Therefore, the assumption of fast motion on the NMR time scale is justified, because at 100 K, $\tau_c \approx 10^{-10}$ s and typical line widths are at most $\Delta \sim 1$ kHz for the carbon CSA and $\Delta \sim 40$ kHz for the second-order quadrupolar interaction of potassium. Consequently, $\tau_c \Delta \ll 1$ at all temperature above 100 K.

Estimation of the ^{13}Carbon CSA with No Proton Disorder. The consistency of our NMR data with the two-sites model developed above was also verified by checking different relationships between δ_{eff} and η_{eff} coming from the properties of the model. First, the product $\delta_{eff}(1 + \eta_{eff}) = \delta(1 + \eta)$ is indeed a constant equal to 84 ppm with standard deviation of 2 ppm, as indicated before from the invariance of δ_{33}. Second, from eqs 6 and 7, δ_{eff} and $\delta_{eff}\eta_{eff}$ should exhibit a linear relationship with F with slopes of, respectively, 0.25 and -0.25. This was verified by the data. With respect to these consistency check, the assumption of a two-site jump seems reasonnable, and we can extract the different unknowns of the model.

The square of the EISF order parameter Δp^2 was recalculated at the temperature of measurement in NMR experiments from the extrapolating function given above, and the function G was plotted as a function of these values. From eq 13, we expect a linear relationship, with a slope equal to $\tan^2(\beta)$ and an intercept at 1. The results appear in Figure 8. The expected linear relationship is found within the experimental uncertainty. The data were fitted with a linear function, either with the intercept fixed at one or used as an adjustable parameter. Both fits represent well the data. As indicated by Figure 8, the G function can be very well fitted by a straight line as a function of Δp^2. To check possible sources of errors coming from temperature calibration or possible misestimation of the square of the order parameter in the EISF experiment, we also checked the correlation between G and different order-parameter functions. All methods give almost the same value of $\tan^2(\beta)$, that is $t = \tan^2(\beta) \approx 1.6 \pm 0.3$, which corresponds to an angle $\beta \approx 52° \pm 3°$. Thus the angle of jump is correctly defined. Because of the inner C_2 symmetry of NMR interaction tensors, the jump angle can be either β or $\pi - \beta$, that is, 52° or 128°.

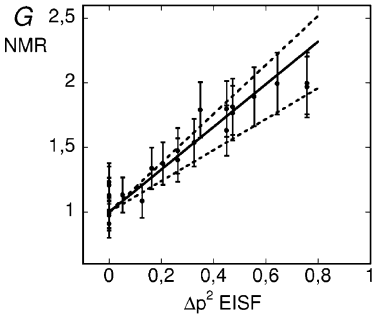

Figure 8. Correlation between the G function defined in eq 13 and the square of the order parameter Δp^2 estimated from the EISF measurements of Eckold. The straight line is the linear best fit excluding the last point (only the slope is adjusted, the intercept was fixed to 1). Dotted lines give an estimation of the incertitude on the slope.

By averaging the data in the high-temperature phase, we obtained $A = F(0,\beta) = \delta(3 - \eta)|\cos(\beta)| \approx 116$ ppm with standard deviation 5 ppm. The average of the smallest eigenvalue gives $B = \delta(1 + \eta) \approx 84 \pm 2$ ppm. Using eq 14 gives the asymmetry parameter $\eta \approx 0.23 \pm 0.08$. Last, the anisotropy is deduced from eq 15 as $\delta \approx 67 \pm 5$ ppm. The largest uncertainty is on the asymmetry parameter. Combining these values with $\delta_{iso} = 161$ ppm gives the *expected chemical shift eigenvalues in the completely ordered state*: $\delta_{11} \approx 228 \pm 6$ ppm, $\delta_{22} \approx 136 \pm 6$ ppm, and $\delta_{33} \approx 119 \pm 2$ ppm.

With these estimations, we can reconstruct the temperature variation of the eigenvalues from eqs 6, 7, and 1−3. The corresponding curves are shown as solid curves on the figures showing the data points (Figures 3 and 4). The agreement is reasonably good for the whole temperature range and indicates that the variation of the asymmetry parameter is very sensitive to the initial value η. It also suggests that the calculated uncertainties may be overestimated, since $\eta = 0.25$ fits well the data.

Discussion of the ^{13}Carbon CSA. To our knowledge, only two ^{13}C CSA powder measurements in $KHCO_3$ appear in the literature.[39,40] These values were obtained at "room temperature" and are compared with the values obtained in this work in Table 1. The small discrepancies between the values of δ_{11} and δ_{22} could be explained by different temperatures because we showed that these eigenvalues are strongly temperature dependent, whereas δ_{33} and δ_{iso} are temperature independent. The values of δ_{iso} are consistent, but the value of δ_{33} quoted by Duncan seems too small. However, δ_{33} compares well with the corresponding values of potassium carbonate ($\delta_{11} = 204$ ppm, $\delta_{22} = 182$ ppm, $\delta_{33} = 122$ ppm) and calcium carbonate ($\delta_{11} = \delta_{22} = 194$ ppm, $\delta_{33} = 119$ ppm).[39]

The effect of hydrogen bonding on the eigenvalues of the chemical shift tensor of carbons belonging to carboxyl group is well documented, and some general trends were deduced from experimental studies.[21−23,39] For instance, in amino acids, the most shielded principal value δ_{33} of the tensor is almost insensitive to the local symmetry of the carboxyl group at 109 ppm versus TMS and found nearly parallel to the normal of the sp^2 plane. The isotropic chemical shift is also rather constant. It is interesting to note that this trend is verified by the majority of the data compiled by Duncan. Thus, the nature of the hydrogen bond cannot be assessed from the knowledge of the isotropic carbon chemical shift alone. This relative insensitivity of these tensor characteristic to the local hydrogen bond structure emphasizes the necessity to study the whole carbon tensor.

TABLE 1: Comparison between the Room-Temperature[a] ^{13}C CSA Eigenvalues Appearing in Literature and from This Work and the Predicted Values with No Proton Disorder

TMS/ppm	*RT* (Stueber[b])	EIM/H-OPT[c] (Stueber[b])	*RT* (Gay[d])	298 K (this work)	$\|\Delta p\| = 1$ (this work)	$318 \leq T \leq 340$ K (this work)
δ_{11}	216	218	218	220	228	211
δ_{22}	145	153	155	143	136	154
δ_{33}	119	117	113	119	119	119
δ_{iso}	160	162.7	162	161	161	161

[a] The exact values of the RT (room temperature) were not specified in the articles. [b] From Stueber et al.[40] [c] Quantum mechanical ab initio calculations with the embedded ion method (EIM) and proton optimization. [d] From Duncan[39] and Gay (unpublished results, 1998).

According to Gu,[21] the least shielded principal value δ_{11} distinguishes protonated ($\delta_{11} > 250$ ppm) and deprotonated forms ($\delta_{11} < 250$ ppm), whereas the intermediate principal value δ_{22} varies widely. Some correlations between δ_{22} and structural data where also proposed. Nevertheless, it seems that the general observed trend is an increase of δ_{11} and a decrease of δ_{22} upon protonation.

The comparison between compounds of different families is difficult. For instance, our measurements on $KHCO_3$ show that the least shielded component δ_{11} is always lower than the corresponding values for protonated carboxyl group in amino acids (which are ~250 ppm). The most shielded principal value δ_{33} (isotropic δ_{iso}) is ~10 ppm higher (lower) than the typical value for amino acids (~170 ppm). But the experimental observed variation of the carboxyl carbon chemical shift eigenvalues of $KHCO_3$ as a function of temperature are completely consistent with the accepted trends explained above. The least shielded δ_{33} and isotropic chemical shift were found to be temperature independent and do not reflect the phase transition. However, δ_{11} decreases and δ_{22} increases as temperature increases, the proton becoming more and more disordered. Such a variation is intuitively equivalent to a modification of the effective protonation state by the change of the population of the different tautomers, as measured by the order parameter (Δp varying between 1 down to 0 when the protonated state diminishes).

Moreover, it also indicates that the rotation of the tensor coupled to the dimer jump occurs around principal axis x_3, which should be roughly perpendicular to the dimer plane.

Obviously, the orientation of the PAS in a reference frame attached to the dimer cannot be deduced from normal powder experiments. However, symmetry consideration may give some hints on the probable CSA PAS orientation. First, the most shielded component δ_{33} was found independent of temperature, that is independent of the order parameter. This result is very important because it indicates that the related common principal axis x_3 is the rotation axis, which is fixed in space. This principal axis x_3 is expected to be perpendicular to the sp^2 COO plane, as in most carboxyl carbons. Let's assume x_3 to be perpendicular to the plane of the four oxygens O_2 and O_3 involved in the hydrogen bonding. In the high-temperature phase where the dimer has symmetry **2/m** with equal $C - O_2$ and $C - O_3$ bond lengths, we expect from symmetry consideration that one principal axis of the averaged CSA tensor bisects the $O_2 - C - O_3$ angle (which is roughly 118°), and that one principal axis is perpendicular to the dimer plane. Thus, in the HT phase, the principal axes x_1 and x_2 are in the dimer plane and parallel to the bisectrix of $O_2 - C - O_3$ (Figure 9). Since the rotation axis x_3 does not change with temperature, it implies that in the LT phase, x_1 and x_2 stay in the dimer plane, and are rotated by $\beta/2$ or $(\pi - \beta)/2$ from the HT direction. Consequently, the principal direction x_1 associated to the least shielded component δ_{11} form an angle $\beta/2 \approx 26°$ or $(\pi - \beta)/2 \approx 64°$ with this mean direction, parallel to the donor/acceptor oxygen direction. In the first case, the x_1 direction would deviate by 33° from one C−O bond and x_2 by 5° from the other C−O bond. In the second case, the deviation angles are the same if we interchange δ_{11} and δ_{22}. Astonishingly, the first case would correspond to the orientation of the carbon CST of the protonated carboxyl group in ammonium hydrogen oxalate hemihydrate. This orientation is also consistent with the empirical trend that the δ_{22} direction is close to the C=O bond.[23]

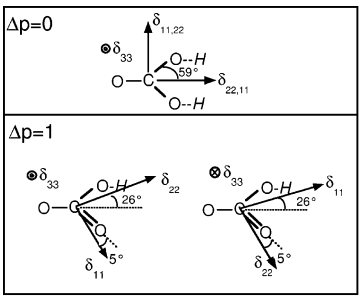

Figure 9. Schematic of our proposal for the possible orientations of the ^{13}C CSA tensor compatible with our data and the local structure of the dimer. Upper part of the figure: HT phase when the dimer has averaged local symmetry 2/*m* and the proton is disordered within a symmetric two-well potential ($\Delta p = 0$); lower part of the figure: completely ordered state $|\Delta p| = 1$. For the sake of clarity, the angles were exaggerated.

Recently, the orientation of the principal axis of the ^{13}C CSA in $KHCO_3$ were predicted by sophisticated ab initio calculation methods using the embedded ion method.[40] The authors found that the principal axis of the most shielded component δ_{33} lies in the molecular plane, as opposed to the usual trend where it was found to be perpendicular to it. However, our results prove that this eigenvalue is not sensitive to the proton disorder, and thus that the corresponding principal axis should be the rotation axis of the tensors. Since the rotation axis is driven by the concerted proton jump, this axis cannot lie in the dimer plane, in contradiction with the above ab initio predictions. However, we would like to remark that two key ingredients were lacking in these ab initio calculations: the dimer structure, and the proton disorder which averages the CSA tensor. (In Table 1, we compare the predicted ab initio eigenvalues to our results. They do not even agree with the unaveraged estimated eigenvalues ($T \rightarrow 0$, as well as with the theoretical bounds.) This could explain the discrepancy between our results and the ab initio predictions of reference.[40] Nevertheless, it is also clear that only single-crystal experiments performed at low temperature (below 100 K) can answer with no ambiguities to the question of the principal axes orientation, as well as that ab initio predictions for hydrogen bonded and ionic compounds should be taken with care.

Discussion of the ^{39}K Potassium Quadrupolar Interaction Tensor. That the phase transition also affects the electric field gradient at the potassium site is not astonishing because $KHCO_3$ is a ionic cristal. The potassium cation K^+ ion has eight neighboring oxygen atoms at ~2.84 Å on average, four of them

with roughly a negative charge $O^{-}{}_{1}$, and four of them directly involved in the dimer hydrogen bonds. Again, we might try to interpret the evolution of the observed quadrupolar interaction with a two-site jump, assuming that the quadrupolar interaction tensor is directly modulated by the stochastic proton jump. By using the same procedure as for the carbon, we estimated the static parameters of the tensor (nuQ $\approx$ 780 kHz, $\eta \approx 0.2$) and the jump angle $\beta \approx 22°$. As indicated by Figure 6, the agreement is correct for the effective asymmetry parameter, but overestimates the reduction of the effective nuQ value, indicating that other effects should be taken into account. Indeed, the two-site jump model is more questionable than for the carbon because the electric field gradient is a long ranged interaction, which is very sensitive to any charge density variation.

Conclusion

The nonferroic phase transition of $KHCO_3$ at ambient pressure was investigated for *the first* time by ^{13}C and ^{39}K solid-state high-resolution NMR within the temperature range $200 \leq T \leq 340$ K. It appears that the anisotropy and asymmetry parameters of the carbon chemical shift and potassium quadrupolar interaction tensors are strongly affected by the phase transition. The most striking results come from the carbon CSA tensor whose largest and middle eigenvalues depend strongly on temperature, whereas the isotropic and smallest eigenvalue are temperature independent within the experimental error, even across the phase transition.

We also revisited the two-site jump model in NMR of an averaged tensor representing the jump of two congruent tensors between two orientations in the fast motion limit and proved the following important equivalence: the smallest eigenvalue of the averaged tensor is independent of probability p if and only if the corresponding principal axis is the rotation axis. A method to obtain the rotation angle, the anisotropy and asymmetry parameters of the static tensors by correlation with other local techniques, such as incoherent neutron scattering, was also proposed.

Using these new results for the two-site model, all the NMR data are interpreted in a consistent manner, by using correlations with another local probe, incoherent neutron scattering. In particular, the evolution of the eigenvalues as a function of temperature was shown to reflect the symmetry breaking due to the phase transition (characterized by the order parameter Δp) through the motional averaging of the corresponding interaction tensors by the protons stochastic motions within the hydrogen bonds of the dimers. It yields an estimation of the eigenvalues of the ^{13}C CSA tensor in $KHCO_3$ when no proton disorder is present, and the jump angle. An orientation of the CSA tensor compatible with the bibliography was also proposed, although it is in contradiction with a recent ab initio prediction.

All these results clearly demonstrate that it is essential to take into account the proton disorder along hydrogen bonds to interpret ^{13}C (or other nuclei whose interactions tensors could be modulated by the proton jump) chemical shift anisotropy, particularly if one is interested in making correlations between the eigenvalues values and local structural information such as bond lengths or angles. Care should also be taken in using quantum mechanical ab initio calculations to predict the principal axes orientations. This work is also another example of the complementarity between two local techniques, high-resolution solid-state NMR and neutron incoherent scattering.

$KHCO_3$ offers the unique opportunity to study the variation of the ^{13}C and ^{39}K interaction tensors as a function of proton disorder (measured by the order parameter Δp). This material is already a model compound for the study of 0-dimensional hydrogen bonds and related phase transitions, but it should also serve as a model compound to test the consistency of ab initio calculations of chemical shifts and electric field gradients. Further work is in progress to understand the relationship between the structures of the compounds of the hydrogen carbonate $XHCO_3$ family, the hydrogen dynamic disorder, and the ionic interaction.

Acknowledgment. I express my sincerest thanks to B. Toudic, M. Buron, and J. Gallier for their constant support and critical reading of the manuscript.

Appendix A

If two congruent tensors T_1 and T_2 have a common principal axis, then they are related by a rotation around this common axis. By congruent tensors, we mean tensors we identical eigenvalues but different principal axes, as should be the case for instance for two sites related by a symmetry operation. It is an obvious result that the corresponding eigenvalue of the *averaged tensor* $<T> = pT_1 + (1 - p)T_2$ is independent of p, whatever the rotation angle. However, it would be also interesting to answer the converse problem: which information are provided about the averaging motion if one of the eigenvalues of the *averaged tensor* is independent of probability p.

In this Appendix, we answer the question if the smallest or largest eigenvalue of the *averaged tensor* formed from the weighted average of congruent tensors remains constant by proving the following result: *the smallest* (*or largest*) *eigenvalue of the averaged tensor* $<T>$ *is independent of* p ***if and only if*** *the rotation axis is the principal axis corresponding to the smallest* (*largest*) *eigenvalue*.

It is worth pointing out the *equivalence* which allow important geometric constraints on the averaging process to be drawn, as discussed in the text. We now prove the result.

Without loss of generality, we can write the averaged tensor in the PAS of one of the tensors as

$$<T>(p) = pD + (1 - p)R^{T}DR \tag{17}$$

where $D = \mathrm{diag}(\lambda_1, \lambda_2, \lambda_3)$ is a diagonal matrix with real eigenvalues $\lambda_1 > \lambda_2 > \lambda_3$. The matrix $\mathbf{R}$ corresponds to the rotation of the principal axes of the second tensor with respect to the principal axes of the first one. $\mathbf{R}$ is an orthogonal matrix satisfying $R^{T}R = \mathbf{I}$ where $\mathbf{I}$ is the unit matrix. To simplify, and because it corresponds to our experimental case, we will suppose that all the eigenvalues of D are strictly different. It is obvious that if the rotation R is around one of the principal axes of the tensor, then the corresponding eigenvalue is invariant. We now want to prove that the converse is also true for the smallest or the largest eigenvalue.

Since $<T>$ is a symmetric real matrix, it can be diagonalized by an orthogonal matrix. Let $\mathbf{w}$ of components w_i be the normalized eigenvector corresponding to the eigenvalue μ of $<T>$, that is $<T>\mathbf{w} = \mu\mathbf{w}$. Note that both the eigenvalue and the eigenvector are functions of probability p. Taking the scalar product of the preceding equation with $\mathbf{w}$, and using the identity

$$p + (1 - p) = p\sum_{i=1}^{3} w_i^{2} + (1 - p)\sum_{i=1}^{3} (\mathbf{Rw})_i^{2} = 1 \tag{18}$$

which is true because both $\mathbf{w}$ and $\mathbf{Rw}$ are normalized vectors

(**R** being an orthogonal matrix, it conserves the scalar norm), we obtain the following equation:

$$\sum_{i=1}^{3}(\lambda_i - \mu)[pw_i^2 + (1-p)(\mathbf{Rw})_i^2] = 0 \qquad (19)$$

We now use the hypothesis that the eigenvalue μ of $< T >$ is equal to the smallest eigenvalue λ_3 of D, whatever the value of p. Then the sum of eq 19 reduces to a two-term sum of *strictly positive terms*. Since the sum should be equal to 0 whatever p, it means that we should have $w_i^2 = 0$ *and* $(\mathbf{Rw})_i^2 = 0$ with $i = 1, 2$. The first condition is equivalent to saying that the corresponding eigenvector is also the third eigenvector of D. The second condition imposes that the rotation R should be performed around this common direction, which means that it is parametrized by only one rotation angle. The theorem is proved.

Note that this proof is also valid if the common invariant eigenvalue is the largest eigenvalue of D, and that the proof also holds whatever the dimension of the matrix D.

References and Notes

(1) Haussühl, S. *Solid State Commun*. **1986**, *57*, 643−647.
(2) Kashida, S.; Yamamoto, K. *J. Solid State Chem.* **1996**, *86*, 180−187.
(3) Kerst, H. Diplomaarbeit, Institut fur Kristallographie RWTH Aachen, 1995.
(4) Wienold, J. Diplomaarbeit, Institut fur Kristallographie RWTH Aachen, 1997.
(5) (a) Takasaka, S.; Tsujimi, Y.; Yagi, T. *Phys. Rev. B* **1997**, *56*, 10715−10718. (b) Takasaka, S.; Tsujimi, Y.; Yagi, T. *J. Korean Phys. Soc*. **1998**, *32* S565−S568.
(6) Legrand, Y.; Rouede, D.; Wienold, J.; Glinnemann, J. *J. Phys. Soc. Jpn* **1998**, *67*, 1451.
(7) Nagai, T., Kagi, H., Yamanaka, T. *Solid State Commun*. **2002**, *123*, 371−374.
(8) Fillaux, F.; Tomkinson, J.; Penfold, J. *Chem. Phys.* **1988**, *124*, 425−437.
(9) Fillaux, F.; Tomkinson, J. *J. Mol. Struct*. **1992**, *270*, 339−349.
(10) Fillaux, F. *Physica D* **1998**, *113*, 172−183.
(11) Fillaux, F. *J. Mol. Struct*. **1999**, *511-512*, 35−47.
(12) Fillaux, F. *Int. Rev. Phys. Chem*. **2000**, *19*, 553−564.
(13) Fillaux, F. *J. Mol. Struct*. **2002**, *615*, 45−59.
(14) Fillaux, F.; Limage, M. H.; Romain, F. *Chem. Phys*. **2002**, *276*, 181−210.
(15) Fillaux, F.; Cousson, A.; Keen, D. *Phys. Rev. B* **2003**, *67*, 054301, 1-10. Fillaux, F.; Cousson, A.; Keen, D. *Phys. Rev. B* **2003**, *67*, 189901.
(16) (a) Thomas, J. O.; Tellgren, R.; Olovsson, I. *Acta Crystallogr*. **1974**, *B30*, 1155−1166.(b) Thomas, J. O.; Tellgren, R.; Olovsson, I. *Acta Crystallogr*. **1974**, *B30*, 2540−2549.
(17) Eckold, G.; Grimm, H.; Stein-Arsic, M. *Physica B* **1992**, *180 & 181*, 336−338.
(18) Neumann, M.; Brougham, D. F.; McGloin, C. J.; Horsewill, A. J.; Trommsdorff, H. P. *J. Chem. Phys.* **1998**, *109*, 7300−7311.
(19) Limbach, H. H. *Magn. Reson. Chem*. **2001**, *39*, S1.
(20) Brunner, E.; Sternberg, U. *J. Prog. Nucl. Magn. Res. Spectrosc*. **1998**, *32*, 21−57.
(21) Gu, Z.; Zambrano, R.; McDermott, A. *J. Am. Chem. Soc*. **1994**, *116*, 6368−6372.
(22) Jagannathan, N. R. *Magn. Reson. Chem.* **1989**, *27*, 941−946.
(23) Veeman, W. S. *Prog. Nucl. Magn. Reson. Spectrosc*. **1984**, *16*, 193−235.
(24) Kempf, J.; Spiess, H. W.; Haeberlen, U.; Zimmermann, H. *Chem. Phys*. **1974**, *4*, 269−276.
(25) Nagaoka, S.; Terao, T.; Imashiro, F.; Saika, A.; Hirota, N.; Hayashi, S. *Chem. Phys. Lett*. **1981**, *80*, 580−584.
(26) Robyr, P.; Meier, B. H.; Ernst, R. R. *Chem. Phys. Lett*. **1991**, *187*, 471−478.
(27) de Dios, A. C. *Prog. Nucl. Magn. Reson. Spectrosc*. **1996**, *29*, 229−278.
(28) Lim, A. R.; Jeong, S. Y. *Phys. Status Solidi B* **2001**, *226*, 413−418.
(29) Feucht, H.; Haeberlen, U.; Pollak-Stachura, M.; Spiess, H. W. *Z. Naturforsch*. **1976**, *31a*, 1173−1180.
(30) (a) Poplett, I. J.; Smith, J. A. S., *J. Chem. Soc., Faraday Trans. 2* **1981**, *77*, 1155−1173. (b) Poplett, I. J.; Smith, J. A. S. *J. Chem. Soc., Faraday Trans. 2* **1981**, *77*, 761−796.
(31) Benz, S.; Haeberlen, U. *J. Magn. Reson*. **1986**, *66*, 125−134.
(32) Cheng, C. P.; Brown, T. L. *J. Am. Chem. Soc*. **1979**, *101*, 2327−2334.
(33) Larcombe-McDouall, J. B.; Smith, J. A. S. *J. Chem. Soc., Faraday Trans. 2* **1989**, *85*, 53−64.
(34) Massiot, D.; Fayon, F.; Capron, M.; King, I.; Le Calv, S.; Alonso, B.; Durand, J.-O.; Bujoli, B.; Gan, Z.; Hoatson, G. *Magn. Reson. Chem*. **2002**, *40*, 70−76.
(35) Detken, A.; Zimmermann, H.; Haeberlen, U.; Luz, Z. *J. Magn. Reson*. **1997**, *126*, 95−102.
(36) Mason, J. *Solid State NMR* **1993**, *2*, 285−288.
(37) Schmidt-Rohr, K., Spiess, H. W. *Multidimensional Solid-State NMR and Polymers*; Academic Press: New York, 1994.
(38) Squires, G. L. *Introduction to the theory of Thermal Neutron Scattering*; Dover Publications: Mineola, NY,,1996; Chapter 4.
(39) Duncan, T. M. *A Compilation of Chemical Shift Anisotropies*; The Farragut Press: Chicago, IL, 1990.
(40) Stueber, D.; Orendt, A. M.; Facelli, J. C.; Parry, R. W.; Grant, D. M. *Sol. State Nucl. Magn. Reson*. **2002**, *22*, 29−49.